Motional quantum states of a trapped ion: Measurement and its back action

S. Wallentowitz and W. Vogel
Arbeitsgruppe Quantenoptik, Fachbereich Physik, Universität Rostock, Universitätsplatz 3, D-18051 Rostock, Germany
(Received 2 April 1996)

We develop a method for reconstructing the quantum mechanical state of a trapped ion by bichromatically irradiating it on a weak electronic transition and subsequently probing a strong electronic transition for resonance fluorescence. Based on this recently proposed scheme [S. Wallentowitz and W. Vogel, Phys. Rev. Lett. **75**, 2932 (1995)] the density matrix of the vibrational motion can be readily obtained either in a generalized position representation or in the number-state representation. The method allows to uniquely define an ultimate classical noise level by a reference measurement with an ion cooled to its vibrational ground-state. Disturbations of the measurement and their suppression are considered. Moreover, we study the effect of the back action of the measurement principle on the motional quantum state. It consists in the splitting of the state to be measured into two substates, giving rise to quantum interference effects. [S1050-2947(96)10710-1]

PACS number(s): 32.80.Pj, 42.50.Vk, 03.65.Bz

I. INTRODUCTION

The experimental realization and observation of a single trapped ion [1] opened new possibilities not only for spectroscopy but also for fundamental tests of quantum physics. In the latter context, quantum jumps have been visualized by recording the intermittent resonance fluorescence from a trapped ion [2–4]. Photon antibunching, for the first time observed in resonance fluorescence from an atomic beam [5], has later been demonstrated with a single trapped ion [6,7]. Moreover, a trapped ion in combination with an appropriate observation technique should allow to detect squeezing in resonance fluorescence [8], an effect that was predicted several years ago [9] but has not been observed yet.

A trapped ion is not only a well defined light source for studying quantum effects of radiation, it also represents an almost ideal object for fundamental experiments in quantum mechanics. The trap potential may be regarded, to a good approximation, as a quantum mechanical harmonic oscillator [10]. Laser sideband cooling allows the preparation of the center-of-mass motion of the ion in the vibrational ground state of the trap potential [11,12]. This is not only of interest for high-resolution spectroscopy, it may also serve as the starting point for the preparation of well defined quantum mechanical states. There exist several proposals for preparing nonclassical quantum states of the ionic center-of-mass motion [13–19]. Recently, number states, squeezed states [20], and Schrödinger-cat-like states of motion [21] have been realized.

Beside the feasibility of studying quantum effects of both the light and the mechanical motion, the trapped ion can be used for dynamical studies of elementary quantum interactions. A vibronic Jaynes-Cummings coupling can be obtained by appropriately irradiating a long-living (e.g., quadrupole) electronic transition of an ion localized within the Lamb-Dicke limit [22]. Beyond the Lamb-Dicke regime, where the spatial extension of the wave function of the vibrational ground state is no longer small compared to the wavelength of the irradiating laser, there even may occur a nonlinear multiquantum Jaynes-Cummings dynamics [23]. This prediction has been confirmed in recent experiments [20]. Such a strongly nonlinear dynamics allows to experimentally realize interesting features of quantum mechanical couplings.

For studying such fundamental effects of quantum mechanics, one important problem must be solved: An appropriate method for measuring the full quantum state of the center-of-mass motion of a trapped ion is desired. For a radiation mode the quantum state has been recorded by optical homodyne tomography [24]. Moreover, the quantum mechanical state of a molecular vibration has been derived from nonstationary spectra of the resonance fluorescence [25]. The latter method, however, can hardly be applied for a trapped ion since its vibronic coupling differs significantly from that of a molecule.

In the present paper we give a detailed study of the method of reconstruction of the motional quantum state proposed by us in Ref. [26]. Besides the reconstruction of the density matrix of the vibrational motion in a generalized position representation, we derive results for the direct sampling of the density matrix in the number-state representation of the harmonic oscillator. Perturbing effects due to imperfections in the detection scheme are studied. Moreover, we analyze the effect of the back action of our measurement principle on the motional quantum state to be measured. This yields an interesting way to prepare nonclassical motional quantum states by the measurement principle. Quantum states obtained in this manner can be measured subsequently by the same technique.

The paper is organized as follows. In Sec. II we describe the measurement principle and derive the electronic dynamics of the trapped ion. The quantum state reconstruction is studied in Sec. III, where the motional density matrix is discussed in two representations, the generalized position representation and the number-state representation. Examples for the measured quantities are given in Sec. IV, where we consider also the disturbing effects due to imperfections of the measurement scheme. The back action of the measurement and its applications are studied in Sec. V. A summary and some conclusions are given in Sec. VI.

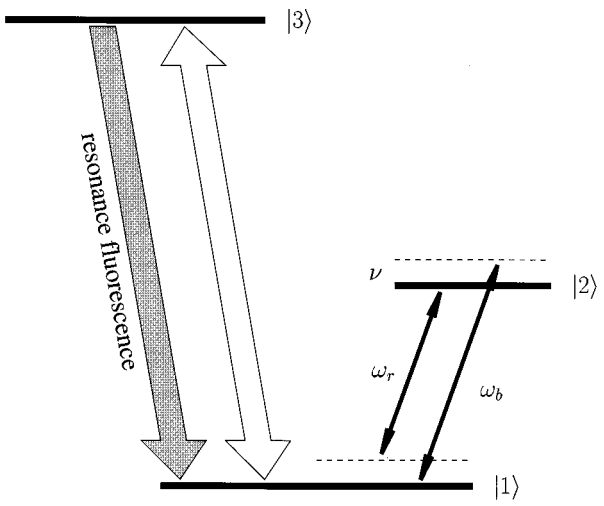

FIG. 1. Scheme of the trapped ion with a weak electronic transition $|1\rangle \Leftrightarrow |2\rangle$ and a strong electronic transition $|1\rangle \Leftrightarrow |3\rangle$. Two incident lasers of frequencies $\omega_b = \omega_{21} + \nu$ and $\omega_r = \omega_{21} - \nu$ are detuned from the electronic transition by the vibrational frequency ν to the blue and red, respectively. The laser driving the strong transition is used for testing the ground-state occupation probabilities $\sigma_{11}(t)$ by means of probing for resonance fluorescence.

II. MEASUREMENT PRINCIPLE

In the following we will show that the quantum mechanical state of a trapped ion can be reconstructed from its electronic dynamics, provided the ion is appropriately irradiated by two laser fields [26]. For this purpose a weak (e.g., quadrupole) electronic transition of the ion is driven by two laser fields, resonant with the well resolved upper and lower vibrational sidebands. For appropriately chosen laser intensities this type of laser excitation results in an interaction Hamiltonian being a product of the electronic transition operators and a generalized position operator $\hat{x}_\varphi$, which depends on the difference phase φ of the two lasers. By measuring the Rabi oscillations of the electronic levels via probing for resonance fluorescence of a second strong transition, one therefore gets information on the generalized spatial distribution for one chosen phase φ. Doing this for all phases, the complete information on the quantum mechanical state of the trapped ion is obtained.

A. Hamiltonian

The excitation scheme of the trapped ion is shown in Fig. 1. The weak transition $|1\rangle \Leftrightarrow |2\rangle$ is irradiated on its well resolved upper and lower first vibrational sidebands by two laser fields of frequencies $\omega_b = \omega_{21} + \nu$ and $\omega_r = \omega_{21} - \nu$, respectively, where $\omega_{21} = \omega_2 - \omega_1$ is the electronic resonance frequency. The trap in which the ion is bound can be described to a good approximation by a harmonic trap potential [10] of vibrational frequency ν. The Hamiltonian for the electronic and vibrational degrees of freedom consists of two parts describing the free evolution $\hat{H}_0$ and the interaction of the ion with the two lasers $\hat{H}_L$ driving its weak transition,

$$\hat{H} = \hat{H}_0 + \hat{H}_L, \tag{1}$$

$$\hat{H}_0 = \hbar \nu \hat{a}^\dagger \hat{a} + \hbar \omega_1 \hat{A}_{11} + \hbar \omega_2 \hat{A}_{22}, \tag{2}$$

$$\hat{H}_L = \lambda E^{(-)}(\hat{x},t)\hat{A}_{12} + \text{H.c.} \tag{3}$$

Here $\hat{a}$ and $\hat{a}^\dagger$ are the annihilation and creation operators of vibrational quanta, respectively, and $\hat{A}_{ab} = |a\rangle\langle b|$ is the electronic flip operator, for the weak transition $|a\rangle \Leftrightarrow |b\rangle$ $(a,b = 1,2)$. The parameter λ determines the coupling strength of the transition with the laser fields, which are resonant to the upper and lower vibrational sidebands of the transition $|1\rangle \Leftrightarrow |2\rangle$,

$$E^{(-)}(\hat{x},t) = E_b e^{i[(\omega_{21}+\nu)t - k_b \hat{x}]} + E_r e^{i[(\omega_{21}-\nu)t - k_r \hat{x}]}. \tag{4}$$

E_b and E_r are the complex amplitudes of the laser fields with phases φ_b and φ_r, respectively. The wave vectors of the two lasers, k_b and k_r, determine the corresponding Lamb-Dicke parameters of the vibrational sideband transitions,

$$k_b \hat{x} = \eta_b(\hat{a}^\dagger + \hat{a}), \quad k_r \hat{x} = \eta_r(\hat{a}^\dagger + \hat{a}), \tag{5}$$

which characterize the localization of the trapped ion with respect to the corresponding laser wavelengths. Note that $\hat{H}_L$ already contains the optical rotating wave approximation, neglecting all terms oscillating in time with the optical frequency ω_{21}. Expanding this Hamiltonian up to first order in the Lamb-Dicke parameters η_b and η_r, which are assumed to be sufficiently small, in the vibrational rotating wave approximation (vibrational frequency ν) the resulting interaction Hamiltonian in the interaction picture reads as

$$\hat{H}_{\text{int}} = -i\lambda(\eta_b E_b \hat{a} + \eta_r E_r \hat{a}^\dagger)\hat{A}_{12} + \text{H.c.} \tag{6}$$

The application of the vibrational rotating wave approximation requires well resolved sidebands of the weak transition.

It is important that the Lamb-Dicke approximation used here is not a serious restriction. It does not exclude the study of motional quantum states containing signatures of nonlinearities in the vibronic coupling beyond the Lamb-Dicke regime [23]. One may get the same interaction Hamiltonian by using Raman-like excitation of the two sidebands [13,16,20,27]. In this case the effective Lamb-Dicke parameters depend on the difference of the wave vectors of the lasers driving each Raman transition. This allows to alter the values of the effective Lamb-Dicke parameters in a wide range, by changing the propagation geometry of the lasers. Therefore, schemes for the preparation of nonclassical quantum mechanical states beyond the Lamb-Dicke regime [18–21] can be used for quantum state preparation using Raman excitations with counterpropagating laser beams. The measurement of these states can be done in the Lamb-Dicke regime by using copropagating beams or an intermediate propagation configuration. In this manner, in Be^+ experiments the Lamb-Dicke parameter can be changed by 6–7 orders of magnitude, values of $\eta = 0.2$ realized in Ref. [20] could be reduced up to $\eta = 10^{-7}$. Moreover, in Ba^+ Lamb-Dicke parameters of $\eta = 10^{-4} \ldots 10^{-5}$ have been realized [28], which could also be enlarged in the above described manner. Therefore, the Lamb-Dicke approximation made in Eq. (6) is not a serious limitation of the method for fundamental applications in the nonlinear domain beyond the Lamb-Dicke regime [29].

Defining complex-valued, effective Rabi frequencies by

$$\Omega=\frac{\lambda}{2\hbar}(\eta_r|E_r|+\eta_b|E_b|)e^{i(\varphi_b+\varphi_r-\pi)/2}, \tag{7}$$

$$\delta\Omega=\frac{\lambda}{2\hbar}(\eta_r|E_r|-\eta_b|E_b|)e^{i(\varphi_b+\varphi_r)/2}, \tag{8}$$

Eq. (6) can be rewritten as

$$\hat{H}_{\rm int}=\hbar(\Omega\hat{A}_{12}+\Omega^*\hat{A}_{21})\hat{x}_\varphi+\hbar(\delta\Omega\hat{A}_{12}+\delta\Omega^*\hat{A}_{21})\hat{x}_{\varphi+\pi/2}. \tag{9}$$

Here we have introduced the generalized, phase dependent position operator of the center-of-mass motion,

$$\hat{x}_\varphi=\hat{a}e^{i\varphi}+\hat{a}^\dagger e^{-i\varphi}. \tag{10}$$

In the Schrödinger picture this operator is the well known phase dependent quadrature operator,

$$\hat{x}_\varphi(t)=\hat{a}e^{i(\varphi+\nu t)}+\hat{a}^\dagger e^{-i(\varphi+\nu t)}. \tag{11}$$

The phase

$$\varphi=(\varphi_b-\varphi_r)/2, \tag{12}$$

can be externally controlled by the phase difference of the two incident laser fields. Since the laser fields can be derived from a single laser by means of acousto-optical modulation, this phase difference is highly stable. The sum phases occurring in the effective Rabi frequencies (7) and (8) in general undergo phase diffusion, so that lasers of small line widths are needed. By using the above mentioned Raman-excitation scheme these phase-diffusion effects are also reduced due to the high level of stability of the phase differences between the Raman beams.

For our method it is important to eliminate the operator $\hat{x}_{\varphi+\pi/2}$ from the interaction Hamiltonian (9). This is done, by fulfilling the condition

$$\eta_b|E_b|=\eta_r|E_r|, \tag{13}$$

where $\delta\Omega$ vanishes and the interaction Hamiltonian is simplified to

$$\hat{H}_{\rm int}=\hbar(\Omega\hat{A}_{12}+\Omega^*\hat{A}_{21})\hat{x}_\varphi. \tag{14}$$

In generalized position representation (for the phase value φ), this Hamiltonian corresponds to a classically driven two-level system with effective Rabi frequency Ωx. The dependence of this effective Rabi-frequency on the generalized position couples in a very simple way the vibrational motion of the ion with its electronic dynamics.

Due to the simple form of this interaction Hamiltonian, the solution of the eigenvalue problem is given by

$$|x;\varphi;\pm\rangle=|x;\varphi\rangle|\pm\rangle, \tag{15}$$

$$\hat{H}_{\rm int}|x;\varphi;\pm\rangle=\pm\hbar|\Omega|x|x;\varphi;\pm\rangle, \tag{16}$$

where the states $|x;\varphi\rangle$ are the eigenstates of the generalized position operator [30],

$$\hat{x}_\varphi|x;\varphi\rangle=x|x;\varphi\rangle, \tag{17}$$

$$|x;\varphi\rangle=\sum_{n=0}^{\infty}\frac{1}{\sqrt[4]{2\pi}}\frac{e^{-in\varphi}}{\sqrt{n!2^n}}H_n\left(\frac{x}{\sqrt{2}}\right)e^{-x^2/4}|n\rangle, \tag{18}$$

with $H_n(x)$ being the Hermite polynomials and the number states $|n\rangle$ being the energy eigenstates of the harmonic trap potential. The electronic eigenstates $|\pm\rangle$ read as

$$(\Omega\hat{A}_{12}+\Omega^*\hat{A}_{21})|\pm\rangle=\pm|\Omega||\pm\rangle, \tag{19}$$

$$|\pm\rangle=\frac{1}{\sqrt{2}}(|1\rangle\pm\frac{\Omega^*}{|\Omega|}|2\rangle). \tag{20}$$

The unitary time evolution due to the interaction with the two lasers is now easily calculated to be

$$\hat{U}_{\rm int}(t)=\int dx|x;\varphi\rangle\langle x;\varphi|[e^{-i|\Omega|xt}|+\rangle\langle+|+e^{i|\Omega|xt}|-\rangle\langle-|]. \tag{21}$$

This time evolution in the interaction picture supplemented by the free time evolution,

$$\hat{U}_0(t)=\hat{U}_{\rm el}(t)\hat{U}_{\rm vib}(t), \tag{22}$$

with

$$\hat{U}_{\rm el}(t)=\exp[-i(\omega_1\hat{A}_{11}+\omega_2\hat{A}_{22})t], \tag{23}$$

$$\hat{U}_{\rm vib}(t)=\exp(-i\nu\hat{a}^\dagger\hat{a}t), \tag{24}$$

determines the whole dynamics, provided the laser intensities are adjusted to fulfil condition (13). The full time evolution operator of the system $\hat{U}(t)$ is then given by

$$\hat{U}(t)=\hat{U}_{\rm el}(t)\hat{U}_{\rm vib}(t)\hat{U}_{\rm int}(t). \tag{25}$$

B. Electronic dynamics

To read out the information on the quantum state of motion in our measurement scheme, the ground-state occupation probability $\sigma_{11}(t)$ is observed. To measure this quantity, the two lasers resonant on the sidebands are switched off at time t and a third laser, exciting a strong dipole transition from the ground state $|1\rangle$ to a third level $|3\rangle$, is used to probe for resonance fluorescence; see Fig. 1. The probabilities for detecting resonance fluorescence, recorded as a function of the interaction time of the two lasers on the weak transition, give the needed ground-state occupation probabilities $\sigma_{11}(t)$. This kind of quantum measurement exhibits a very high quantum efficiency, so that efficiency problems, as known from optical homodyne tomography [24] and from quantum state measurements of molecular vibrations [25], do not occur.

The initial state of the ion $\hat{\varrho}(0)$ is assumed to be a decorrelated one of the form

$$\hat{\varrho}(0)=\hat{\rho}(0)\otimes\hat{\sigma}(0), \tag{26}$$

where the electronic density operator $\hat{\sigma}(0)$ is given by

$$\hat{\sigma}(0)=\sum_{a,b=1,2}\sigma_{ab}(0)|a\rangle\langle b|, \tag{27}$$

$\sigma_{11}(0)$ being the initial ground-state occupation and $\sigma_{12}(0)$ being the initial electronic coherence. The quantum mechanical state of the vibrational motion of the trapped ion is described by the initial density operator $\hat{\rho}(0)$. With the help of Eqs. (21)–(25), the ground-state occupation probability after an interaction time t reads as

$$\begin{aligned}\sigma_{11}(t)&=\mathrm{Tr}[|1\rangle\langle 1|\hat{\varrho}(t)]\\&=\mathrm{Tr}[|1\rangle\langle 1|\hat{U}_{\mathrm{int}}(t)\hat{\varrho}(0)\hat{U}_{\mathrm{int}}^{\dagger}(t)],\end{aligned} \tag{28}$$

where the symbol Tr denotes the trace over both the vibrational and the electronic degrees of freedom. After some straightforward calculation one finally obtains

$$\begin{aligned}\sigma_{11}(\tau;\varphi)-\frac{1}{2}=\int dx\, e^{ix\tau}\Bigg\{\left[\sigma_{11}(0)-\frac{1}{2}\right]p_s(x;\varphi)\\+i\mathrm{Re}[\sigma_{12}(0)e^{-i(\varphi_b+\varphi_r)/2}]p_a(x;\varphi)\Bigg\},\end{aligned} \tag{29}$$

where τ is the dimensionless time,

$$\tau=2|\Omega|t. \tag{30}$$

Note that σ_{11} depends on the chosen phase value φ (characterizing the representation used) as a parameter. For convenience we have introduced the symmetrized and antisymmetrized spatial probability densities,

$$p_s(x;\varphi)=\frac{1}{2}[p(x;\varphi)+p(-x;\varphi)], \tag{31}$$

$$p_a(x;\varphi)=\frac{1}{2}[p(x;\varphi)-p(-x;\varphi)], \tag{32}$$

with

$$p(x;\varphi)=\langle x;\varphi|\hat{\rho}(0)|x;\varphi\rangle, \tag{33}$$

being the probability to find the ion at the generalized position x for the chosen phase value φ. While the first integrand in Eq. (29) is insensitive to coherences of the initial electronic state of the ion, the second integrand in Eq. (29) gives contributions solely due to a coherent electronic preparation of the ion.

III. QUANTUM STATE RECONSTRUCTION

In the preceding section we have shown that the ground-state occupation probabilities $\sigma_{11}(\tau;\varphi)$ of a bichromatically driven trapped ion contains the full information on the probability distribution $p(x;\varphi)$ for the generalized position x at a given phase φ. This information is recorded, with a very high quantum efficiency, by probing a strong electronic transition of the ion for resonance fluorescence. In this section these results will be used to reconstruct the motional density matrix of the trapped ion.

A. Generalized position representation

The ground-state occupation probabilities (29) are determined by the initial, phase dependent spatial distributions of the trapped ion. This allows to reconstruct the quantum mechanical state of the trapped ion in a generalized position representation. To reconstruct the spatial distribution $p(x;\varphi)$ from the measured ground-state occupation probabilities $\sigma_{11}(\tau;\varphi)$ we can separate the contributions $p_s(x;\varphi)$ and $p_a(x;\varphi)$ in Eq. (29) by two independent measurements of $\sigma_{11}(\tau;\varphi)$, with incoherently and coherently prepared initial electronic states. The latter can be achieved by prepumping the ion with a laser tuned to the pure electronic resonance of the weak transition.

An *incoherent measurement* with an initial preparation of the ion in its electronic ground-state,

$$\sigma_{11}(0)=1, \tag{34}$$

yields the symmetrized spatial distribution $p_s(x;\varphi)$,

$$\sigma_{11}^{(\mathrm{inc})}(\tau;\varphi)-\frac{1}{2}=\frac{1}{2}\int dx\, e^{ix\tau}p_s(x;\varphi). \tag{35}$$

Performing an additional *coherent measurement*, for example, with the electronic preparation [31]

$$\sigma_{11}(0)=|\sigma_{12}(0)|=\frac{1}{2},\quad \arg[\sigma_{12}(0)]=\frac{\varphi_b+\varphi_r}{2}\pm\pi, \tag{36}$$

allows one to derive the antisymmetrized spatial distribution $p_a(x;\varphi)$,

$$\sigma_{11}^{(\mathrm{coh})}(\tau;\varphi)-\frac{1}{2}=-\frac{i}{2}\int dx\, e^{ix\tau}p_a(x;\varphi). \tag{37}$$

Combining both results we can relate the characteristic function $\Psi(\tau;\varphi)$ of the generalized spatial distribution,

$$\Psi(\tau;\varphi)=\int dx\; e^{ix\tau}p(x;\varphi), \tag{38}$$

directly to the measured fluorescence signal, via

$$\Psi(\tau;\varphi)=2\left[\sigma_{11}^{(\mathrm{inc})}(\tau;\varphi)-\frac{1}{2}\right]+2i\left[\sigma_{11}^{(\mathrm{coh})}(\tau;\varphi)-\frac{1}{2}\right]. \tag{39}$$

This function, known for an interval of the phase φ of size π, provides the full information on the quantum mechanical state of the ionic center-of-mass motion.

Applying results for the reconstruction of the density matrix of a radiation mode in a field-strength basis [32], we may relate the density matrix in generalized position representation to a twofold Fourier transform of the spatial distribution as follows:

$$\langle x+\delta x;\varphi|\hat{\rho}(0)|x-\delta x;\varphi\rangle = \frac{1}{2\pi}\int ds\, e^{-ixs}\int dx' e^{ix'\sqrt{s^2+\delta x^2}} p\left(x';\varphi+\frac{\pi}{2} - \arg(is-\delta x)\right). \tag{40}$$

Since the first Fourier integral with respect to x' in Eq. (40) can be identified as the characteristic function $\Psi(\tau;\varphi)$,

$$\Psi\left[\sqrt{s^2+\delta x^2};\varphi+\frac{\pi}{2}-\arg(is-\delta x)\right] = \int dx' e^{ix'\sqrt{s^2+\delta x^2}} p\left(x';\varphi+\frac{\pi}{2}-\arg(is-\delta x)\right), \tag{41}$$

the density matrix in generalized position representation can be obtained by a simple Fourier transform of the measured characteristic function given in Eq. (39),

$$\langle x+\delta x;\varphi|\hat{\rho}(0)|x-\delta x;\varphi\rangle = \frac{1}{2\pi}\int_{-\infty}^{+\infty} ds\, e^{-ixs}\Psi[\tau(s,\delta x);\varphi(s,\delta x)], \tag{42}$$

where the parameterized time and phase are

$$\tau(s,\delta x)=\sqrt{s^2+\delta x^2}, \tag{43}$$

$$\varphi(s,\delta x)=\varphi+\frac{\pi}{2}-\arg(is-\delta x). \tag{44}$$

Whereas in optical homodyne tomography $p(x;\varphi)$ corresponds to the measured quantity [24], in our scheme we record the first Fourier transform in Eq. (40), that is, the characteristic function $\Psi(\tau;\varphi)$. This simplifies the reconstruction procedure of the density matrix to only a single Fourier transform of the measured data.

Another possibility to construct the characteristic function $\Psi(\tau;\varphi)$ out of measured data is to use only one kind of electronic preparation and to measure with this initial preparation at the two different phases. To see this one can calculate the following observables:

$$\sigma_{11}^{(+)}(\tau;\varphi)=\frac{1}{2}[\sigma_{11}(\tau;\varphi+\pi)+\sigma_{11}(\tau;\varphi)], \tag{45}$$

$$\sigma_{11}^{(-)}(\tau;\varphi)=\frac{1}{2}[\sigma_{11}(\tau;\varphi+\pi)-\sigma_{11}(\tau;\varphi)], \tag{46}$$

which are derived from the ground-state occupation probabilities measured at the two phases φ and $\varphi+\pi$, with identical values of $\sigma_{11}(0)$ and $\mathrm{Re}[\sigma_{12}(0)e^{-i(\varphi_b+\varphi_r)/2})]$ for both measurements.

These measured quantities can be related, following Eq. (29), to the symmetrized and antisymmetrized spatial probability densities by

$$\sigma_{11}^{(+)}(\tau;\varphi)-\frac{1}{2}=\left[\sigma_{11}(0)-\frac{1}{2}\right]\int dx\, e^{ix\tau}p_s(x;\varphi), \tag{47}$$

$$\sigma_{11}^{(-)}(\tau;\varphi)-\frac{1}{2} = -i\mathrm{Re}[\sigma_{12}(0)e^{-i(\varphi_b+\varphi_r)/2}]\int dx\, e^{ix\tau}p_a(x;\varphi), \tag{48}$$

provided the initial electronic preparation is appropriately chosen so that the prefactors on the right-hand sides of Eqs. (47) and (48) do not vanish.

Following Eqs (35), (37), (47), and (48), the relations between the two kinds of measuring the ground-state occupation probabilities read as

$$\sigma_{11}^{(\mathrm{inc})}(\tau;\varphi)-\frac{1}{2}=\frac{1}{2\left[\sigma_{11}(0)-\frac{1}{2}\right]}\left[\sigma_{11}^{(+)}(\tau;\varphi)-\frac{1}{2}\right], \tag{49}$$

$$\sigma_{11}^{(\mathrm{coh})}(\tau;\varphi)-\frac{1}{2} = \frac{1}{2\mathrm{Re}[\sigma_{12}(0)e^{-i(\varphi_b+\varphi_r)/2}]}\left[\sigma_{11}^{(-)}(\tau;\varphi)-\frac{1}{2}\right], \tag{50}$$

so that in Eq. (39) and in the following, $\sigma_{11}^{(\mathrm{inc/coh})}(\tau;\varphi)$ could be replaced by $\sigma_{11}^{(\pm)}(\tau;\varphi)$.

B. Number-state representation

An alternative approach to reconstruct the density matrix is the use of the number-state basis. In this representation, a direct sampling procedure of the density matrix of light from optical homodyne tomography has been developed in a series of papers [33]. In our scheme the outcome of each probing for resonance fluorescence can be also directly mapped into the density matrix. For this purpose one may apply Eq. (18) to get the following expressions for the symmetrized and antisymmetrized spatial probability densities

$$p_s(x;\varphi)=e^{-x^2/2}\sum_{n,k}\frac{e^{-i2k\varphi}}{2^{n+k+\frac{1}{2}}\sqrt{\pi n!(n+2k)!}} \times H_n\left(\frac{x}{\sqrt{2}}\right)H_{n+2k}\left(\frac{x}{\sqrt{2}}\right)\rho_{n,n+2k}, \tag{51}$$

$$p_a(x;\varphi)=e^{-x^2/2}\sum_{n,k}\frac{e^{-i(2k+1)\varphi}}{2^{n+k+1}\sqrt{\pi n!(n+2k+1)!}} \times H_n\left(\frac{x}{\sqrt{2}}\right)H_{n+2k+1}\left(\frac{x}{\sqrt{2}}\right)\rho_{n,n+2k+1}, \tag{52}$$

where we have used the motional density matrix in number-state representation,

$$\rho_{m,n}=\langle m|\hat{\rho}(0)|n\rangle. \tag{53}$$

Inserting Eqs. (51) and (52) in Eqs. (35) and (37) we may relate the measurable ground-state occupation probabilities to the density matrix in number-state representation,

$$\sigma_{11}^{(\mathrm{inc})}(\tau;\varphi)-\frac{1}{2}=-e^{-\tau^2/2}\sum_{n,k}\sqrt{\frac{n!}{(n+2k)!}}(-2)^{k-1}\times e^{-i2k\varphi}\left(\frac{\tau}{\sqrt{2}}\right)^{2k}L_n^{(2k)}(\tau^2)\rho_{n,n+2k}, \tag{54}$$

$$\sigma_{11}^{(\mathrm{coh})}(\tau;\varphi)-\frac{1}{2}=e^{-\tau^2/2}\sum_{n,k}\sqrt{\frac{n!}{(n+2k+1)!}}(-2)^{k}\times e^{-i(2k+1)\varphi}\left(\frac{\tau}{\sqrt{2}}\right)^{2k+1}L_n^{(2k+1)}(\tau^2)\times\rho_{n,n+2k+1}, \tag{55}$$

with $L_n^{(k)}(x)$ being the Laguerre polynomials. By Fourier integrating over the phase φ and using the orthogonality relation of the Laguerre polynomials [34] one finally obtains

$$\rho_{n,n+k}=\int_0^{\pi}d\varphi\, e^{ik\varphi}\int_0^{\infty}d\tau\,\mathcal{S}_n^{(k)}(\tau)\times\begin{cases}\sigma_{11}^{(\mathrm{inc})}(\tau,\varphi)-\frac{1}{2} & \text{for } k\geq 0,\ k \text{ even}\\ \sigma_{11}^{(\mathrm{coh})}(\tau,\varphi)-\frac{1}{2} & \text{for } k\geq 0,\ k \text{ odd.}\end{cases} \tag{56}$$

The elements of the density matrix for $k<0$ are obtained from the symmetry relation

$$\rho_{n+k,n}=\rho_{n,n+k}^{*}. \tag{57}$$

The sampling functions $\mathcal{S}_n^{(k)}(\tau)$ are explicitly given by

$$\mathcal{S}_n^{(k)}(\tau)=\frac{4}{\pi}\sqrt{\frac{2n!}{(n+k)!}}\left(\frac{\tau}{\sqrt{2}}\right)^{k+1}L_n^{(k)}(\tau^2)e^{-\tau^2/2}\times\begin{cases}(-2)^{k/2} & \text{for } k\geq 0,\ k \text{ even}\\ (-2)^{(k-1)/2} & \text{for } k\geq 0,\ k \text{ odd.}\end{cases} \tag{58}$$

These sampling functions can be easily calculated using the recursion relation with respect to n,

$$\sqrt{n(n+k)}\,\mathcal{S}_n^{(k)}(\tau)=(2n+k-\tau^2-1)\mathcal{S}_{n-1}^{(k)}(\tau)-\sqrt{(n-1)(n+k-1)}\,\mathcal{S}_{n-2}^{(k)}(\tau), \tag{59}$$

and a recursion relation with respect to k ($k\geq 0$),

$$\mathcal{S}_0^{(k)}(\tau)=-\frac{\tau^2}{\sqrt{k(k-1)}}\mathcal{S}_0^{(k-2)}(\tau), \tag{60}$$

with the special values for $n=0$ and $k=0,1$ being

$$\mathcal{S}_0^{(0)}(\tau)=\frac{4\tau}{\pi}e^{-\tau^2/2}, \tag{61}$$

$$\mathcal{S}_0^{(1)}(\tau)=\frac{4\tau^2}{\pi\sqrt{2}}e^{-\tau^2/2}. \tag{62}$$

In view of the fact that one measures directly the characteristic function $\Psi(\tau;\varphi)$ and not the spatial distribution $p(x;\varphi)$, the sampling functions (58) are much simpler than in the case of optical homodyne tomography [33,35]. By multiplying the sampling functions $e^{ik\varphi}\mathcal{S}_n^{(k)}(\tau)$ with the outcome of each probing for resonance fluorescence (*on* ⇔ *off*) at various times τ and phases φ and mapping these contributions into the density matrix elements $\rho_{n,n+k}$, the reconstruction has been done after the processing of a sufficient large number of events.

If one is only interested in the motional number statistics, $P_n=\rho_{n,n}$, Eq. (56) is reduced to

$$P_n=\frac{2}{\pi}\int_0^{\pi}d\varphi\int_0^{\infty}d\tau^2 e^{-\tau^2/2}L_n(\tau^2)\left[\sigma_{11}^{(\mathrm{inc})}(\tau;\varphi)-\frac{1}{2}\right]. \tag{63}$$

This result is valid for any quantum state of the vibrational motion of the trapped ion. It can be further simplified for completely incoherent superpositions of number states, that is, for situations where the full information on the motional quantum state is contained in its number statistics P_n,

$$\hat{\rho}(0)=\sum_{n=0}^{\infty}P_n|n\rangle\langle n|. \tag{64}$$

In such cases $\sigma_{11}^{(\mathrm{coh})}(\tau;\varphi)-1/2$ vanishes and $\sigma_{11}^{(\mathrm{inc})}(\tau;\varphi)$ is phase independent. This situation is expected to appear in standard laser-cooling experiments. From Eqs. (63) and (64) we find

$$P_n=2\int_0^{\infty}d\tau^2 e^{-\tau^2/2}L_n(\tau^2)\left[\sigma_{11}^{(\mathrm{inc})}(\tau)-\frac{1}{2}\right]. \tag{65}$$

In the particular case where the state is a thermal one, the statistics reads as

$$P_n=(1-e^{-\beta})e^{-\beta n}, \tag{66}$$

with $\beta=\hbar\nu/k_BT$, T being the temperature of the motional degree of freedom and k_B being the Boltzmann constant. Our detection scheme renders is possible to rigorously check whether the motional state fulfills the conditions (64) and (66). If it does, the temperature T can be easily determined. To show this we insert the thermal statistics (66) in Eq. (54) and obtain

$$\sigma_{11}^{(\mathrm{inc})}(\tau)-\frac{1}{2}=\frac{1}{2}\exp\left[-\frac{\tau^2}{2(1-e^{-\beta})}\right]. \tag{67}$$

From this we readily obtain the relation between the exponential decay time τ_e, defining the exponential decay of the quantity $\sigma_{11}^{(\mathrm{inc})}(\tau)-1/2$, and the temperature T,

$$T=\frac{\hbar\nu}{k_B}\left[\ln\left(\frac{2+\tau_e^2}{2-\tau_e^2}\right)\right]^{-1}. \tag{68}$$

The temperature T of the ionic center-of-mass motion is related to the mean thermal number of vibrational quanta, $n_{\rm th}$, as follows:

$$n_{\rm th}=\left[\exp\left(\frac{\hbar\nu}{k_BT}\right)-1\right]^{-1}. \tag{69}$$

In terms of the decay time τ_e it is given by

$$n_{\rm th}=\frac{2-\tau_e^2}{2\tau_e^2}. \tag{70}$$

IV. FLUORESCENCE SIGNAL FOR PARTICULAR QUANTUM STATES

Let us now consider some examples for the resonance fluorescence signal which can be recorded in experiments, reflecting the different initial quantum states of the center-of-mass motion of the ion. In Sec. IV A we will consider some examples for the situation of our measurement scheme when the Hamiltonian (14) applies. The case when the matching of the laser fields according to Eq. (13) is imperfect, so that the full Hamiltonian (9) must be used, is studied in Sec. IV B.

A. Perfect scheme

First of all let us deal with the dynamics of the fluorescence signal for thermal states. In Fig. 2(a) the symmetrized spatial distributions are shown for the vibrational ground state and for thermal states with $n_{\rm th}=1$ and $n_{\rm th}=4$. Since the dynamics of the electronic ground-state occupation probability $\sigma_{11}(\tau;\varphi)$ is related by Fourier transform to the generalized position distribution $p(x;\varphi)$, the widths of these distributions determine the decay times of the measured signal; see Fig. 2(b). Therefore the decays of the resonance fluorescence signal become the faster the larger the temperatures are, as described by Eq. (68). Due to the larger widths of their spatial distributions, for any thermal state the fluorescence signals decay faster than for the vibrational ground state.

For coherent states the widths of the spatial distributions are equal to that of the vibrational ground state; see Fig. 3(a). In these particular cases the decay times are always the same and the fluorescence signals oscillate with frequencies determined by the amplitudes of the coherent states; see Fig. 3(b). The decay for the vibrational ground state given in Fig. 3(b) represents an envelope, containing all states for which the widths of their spatial structures are equal or larger than that of the ground state. Since nonclassical states usually exhibit structures in their distribution $p(x;\varphi)$ which are narrower than the spatial ground-state distribution, the vibrational ground-state decay may be regarded as a boundary between classical and nonclassical behavior of the motional quantum states of the trapped ion. Any quantum state which exhibits in our detection scheme a fluorescence signal with a dynamics beyond this boundary has some spatial structures narrower than that of the vibrational ground state, and may be considered as a nonclassical motional quantum state of the ion. To determine this boundary between classical and quantum mechanics one has to measure the fluorescence signals of a laser-cooled ion, which may represent to a very good approximation an ion in the vibrational ground state [12]. Figure 4 shows the fluorescence signal for a coherent vibrational state in dependence on the phase φ. At the phase value $\varphi=\pi/2$ the ground-state decay can be seen. For this phase the spatial distribution corresponds to that of the ground state, since the coherent state is chosen to have a real-valued amplitude.

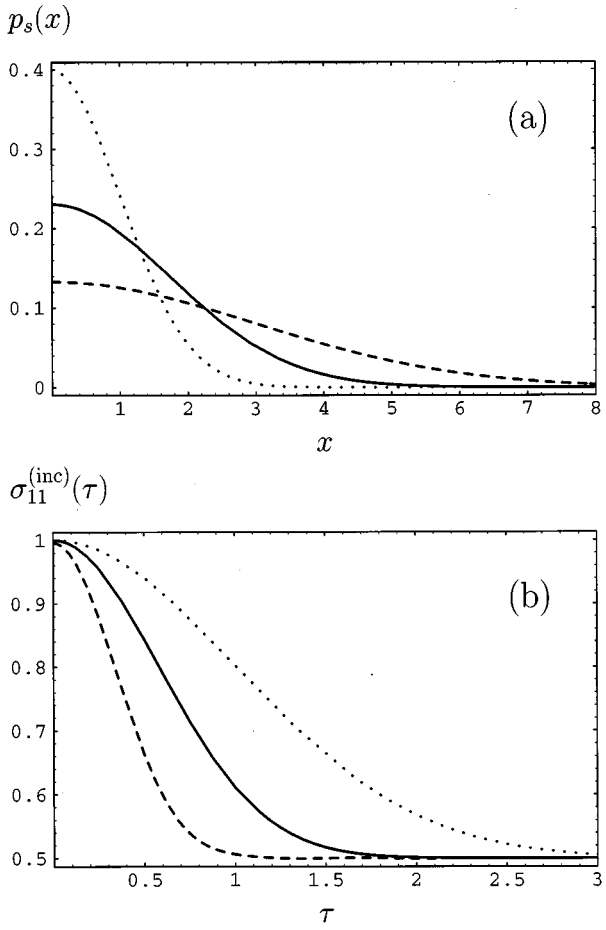

FIG. 2. Symmetrized spatial distributions (a) and incoherent ground-state occupation probabilities (b) for thermal states with $n_{\rm th}=1$ (solid), $n_{\rm th}=4$ (dashed), and for the vibrational ground state (dotted). The temperature of the vibrational motion determines the decay time of the fluorescence signal.

Examples for nonclassical quantum states with structures narrower than those of the ground-state are considered in Figs. 5 and 6, where the fluorescence signal shows a dynamics beyond the ground-state envelope. This is illustrated in Fig. 5 for a number state and for an even coherent state (Schrödinger-cat state). Figure 6 shows the phase-dependent incoherent ground-state occupation probability for even and odd coherent states of atomic motion [18,21]. One observes signatures for a nonclassical behavior around the phase value $\varphi=\pi/2$, where even and odd coherent states can be easily distinguished by their long-time dynamics. These long-time structures in $\sigma_{11}^{(\rm inc)}(\tau;\varphi)$ are a direct reflection of the quantum interference fringes of the states in $p(x;\varphi)$, which exhibit structures narrower than the ground-state distribution. In our scheme these effects can be easily recorded without

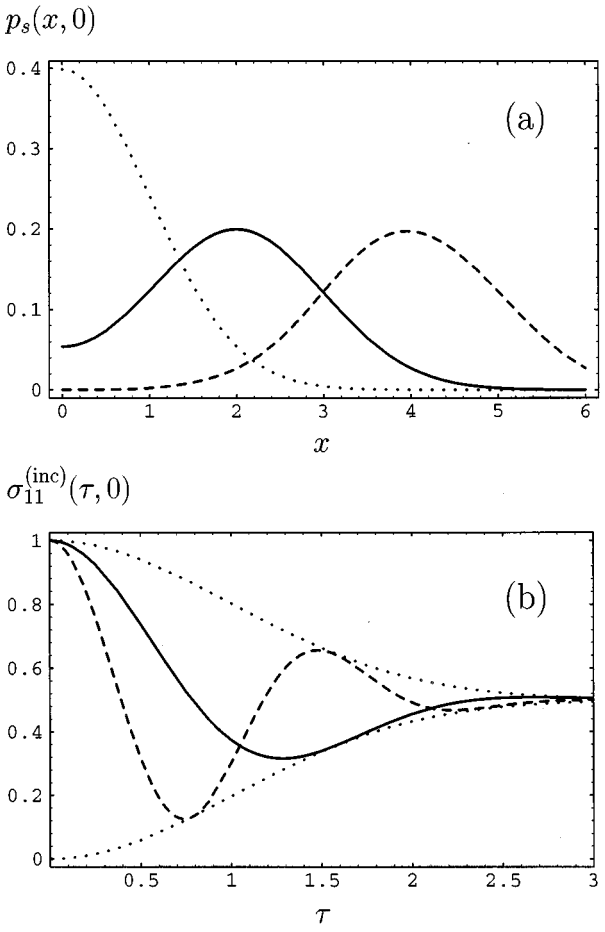

FIG. 3. Symmetrized spatial distributions (a) and incoherent ground-state occupation probabilities (b) for coherent states with amplitudes $\alpha=1$ (solid), $\alpha=2$ (dashed), and for the vibrational ground state corresponding to $\alpha=0$ (dotted), considered for the phase $\varphi=0$. Due to the same spatial widths the decay times are equal.

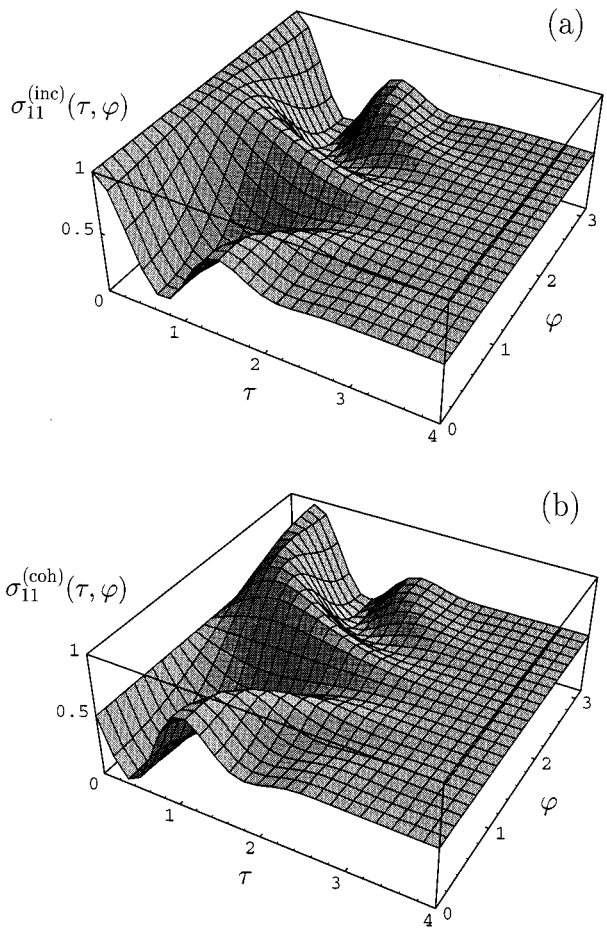

FIG. 4. Phase-dependent incoherent (a) and coherent (b) ground-state occupation probabilities for a coherent state of amplitude $\alpha=2$.

requirements of high resolution: The sharper the fringes are, the slower is the dynamics.

For the quantum states under consideration, the coherently prepared measurements yield for all phases and times a probability of 1/2 to observe a fluorescence signal. This is due to the fact that the number states and the even and odd coherent states have a symmetric spatial distribution ($x \Leftrightarrow -x$). In other words, their density matrix elements $\rho_{n,n+k}$ are zero for odd k. In more general cases, the determination of the antisymmetric distributions must be performed to get the full information on the quantum state to be measured.

B. Mismatch of the laser intensities

An important assumption of our measurement principle is that the intensities of the lasers fulfill condition (13). If this is not the case one gets a mismatch leading to nonvanishing values of $\delta\Omega$ in the Hamiltonian (9). The additional term in the Hamiltonian includes the momentumlike operator $\hat{x}_{\varphi+\pi/2}$ in the dynamics of the system. Due to this contribution one gets a modification of the measured ground-state probabilities depending on the relative strength of the mismatch $\delta\Omega/\Omega$ and on the quantum state under study.

The temporal behavior of the fluorescence signal for an ion prepared in the vibrational ground state depends crucially on the intensity mismatch; see Fig. 7. In an experiment this sensitivity enables one to accurately calibrate the two laser intensities to fulfill condition (13) by measuring the resonance fluorescence probabilities of a known motional quantum state. By laser cooling the ion, one can presently reach the vibrational ground state $|0\rangle$ with a probability of about 98% [12]. An ion prepared in this manner can be used as a reference state and the dynamics of the corresponding fluorescence signal can be compared with the expected result for $\delta\Omega=0$. Varying the ratio of the laser strengths to get an agreement of the measured values with the calculated ones for a rather long time scale, one can precisely calibrate the measurement apparatus to fulfill Eq. (13). In Fig. 8 the modifications of the fluorescence signal due to intensity mismatch are shown for an even coherent state. Obviously, the magnitude of the mismatch effects is seen to depend on the quantum state to be measured. It appears that a relative accuracy of matching the intensities of 10^{-3} already gives suitable results. Note that the fields can be derived by acousto-optical

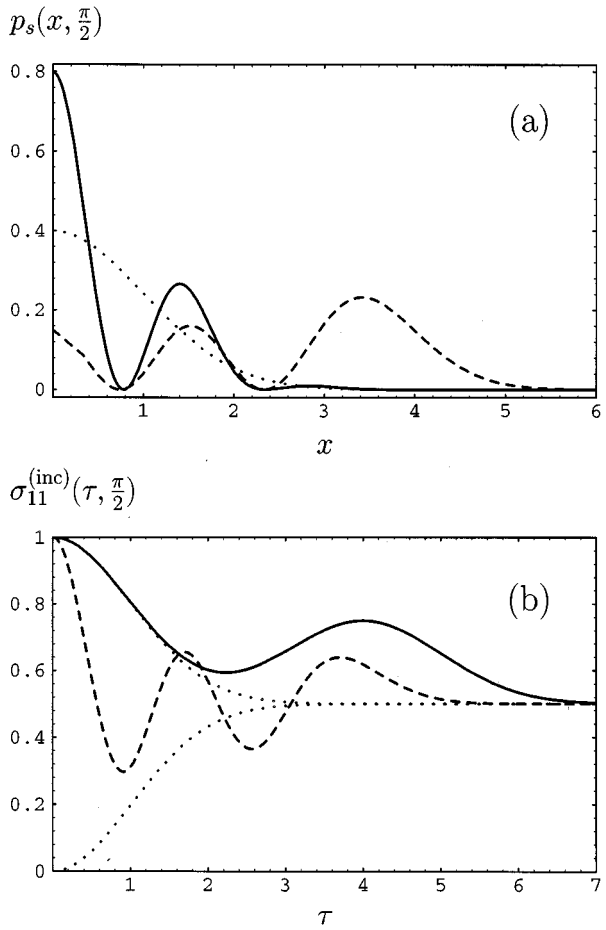

FIG. 5. Symmetrized spatial distributions (a) and incoherent ground-state occupation probabilities (b) for nonclassical states in comparison with the vibrational ground state (dotted): even coherent state (Schrödinger-cat state) with $\alpha=2$ (solid) and number state with $n=4$ (dashed). The nonclassical properties are seen in the long-time dynamics of the fluorescence signal beyond that of the vibrational ground-state envelope.

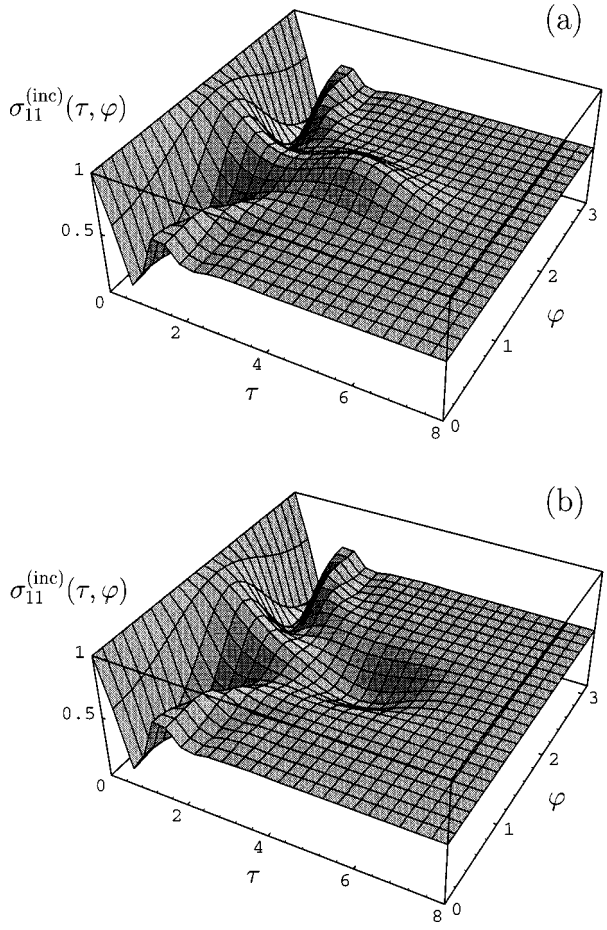

FIG. 6. Phase-dependent incoherent ground-state occupation probabilities for even (a) and odd (b) coherent states with $\alpha=2$. A signature for the nonclassical properties of these states are the long-time dynamics around the phase-value $\varphi=\pi/2$.

modulation from a single laser, which allows a high precision of matching.

V. BACK ACTION OF THE MEASUREMENT

In the previous sections we have shown that the proposed measurement scheme is able to obtain the complete information on the quantum mechanical state of the trapped ion. The measurement allows one to determine an initially prepared ionic vibrational quantum state, which evolves due to the interaction with the two lasers into a new quantum state. By probing for resonance fluorescence at time t this state will be further modified. To see this back action of the measurement, let us consider the electronic matrix elements $\langle a|\hat{U}_{\mathrm{int}}(t)|b\rangle$ of the time evolution operator (interaction part), which are still operators in the motional degree of freedom. Based on Eq. (14) it reads as

$$\langle a|\hat{U}_{\mathrm{int}}(t)|b\rangle=\langle a|\exp[-i(\Omega\hat{A}_{12}+\Omega^*\hat{A}_{21})\hat{x}_\varphi t]|b\rangle, \tag{71}$$

with $a,b=1,2$. For equal electronic states ($a=b$) this operator reads as

$$\langle a|\hat{U}_{\mathrm{int}}(t)|a\rangle=\sum_{n=0}^{\infty}(-i)^n\frac{(\hat{x}_\varphi t)^n}{n!}\langle a|(\Omega\hat{A}_{12}+\Omega^*\hat{A}_{21})^n|a\rangle$$

$$=\frac{1}{2}(e^{-i\hat{x}_\varphi\tau/2}+e^{i\hat{x}_\varphi\tau/2}), \tag{72}$$

where τ is given in Eq. (30). For different electronic levels ($a\neq b$) one gets in the same manner

$$\langle 1|\hat{U}_{\mathrm{int}}(t)|2\rangle=\frac{\Omega}{2|\Omega|}(e^{-i\hat{x}_\varphi\tau/2}-e^{i\hat{x}_\varphi\tau/2}), \tag{73}$$

$$\langle 2|\hat{U}_{\mathrm{int}}(t)|1\rangle=\frac{\Omega^*}{2|\Omega|}(e^{-i\hat{x}_\varphi\tau/2}-e^{i\hat{x}_\varphi\tau/2}). \tag{74}$$

Since the coherent displacement operator of the vibrational motion is defined as

$$\hat{D}(\alpha)=\exp(\alpha\hat{a}^\dagger-\alpha^*\hat{a}), \tag{75}$$

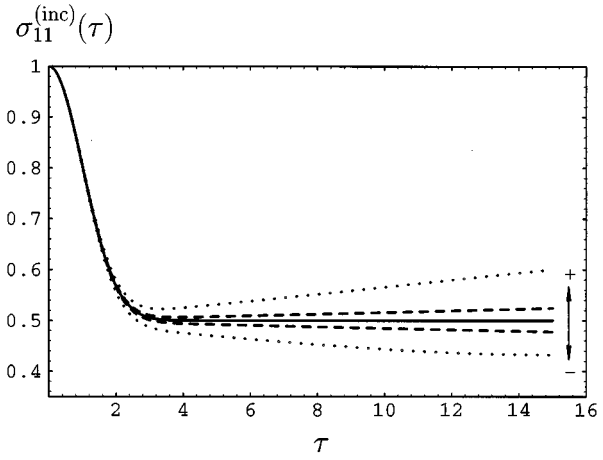

FIG. 7. Deviations from the perfect dynamics (solid) due to laser intensity mismatch, for the ion being prepared in the vibrational ground state. Mismatch parameters: $|\delta\Omega|/|\Omega| = \pm 0.25\%$ (dashed) and $|\delta\Omega|/|\Omega| = \pm 1\%$ (dotted).

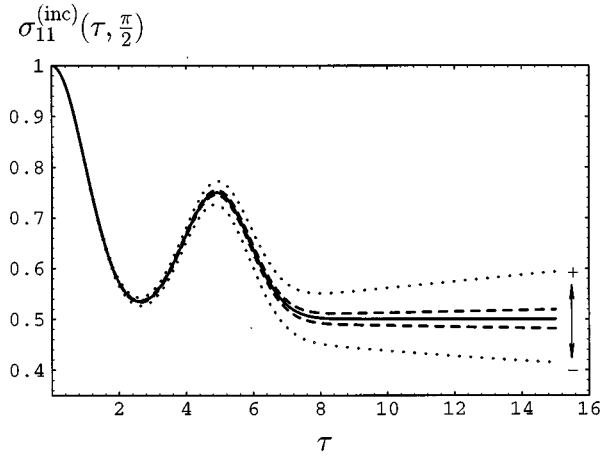

FIG. 8. Deviations from the perfect dynamics (solid) due to laser intensity mismatch for a nonclassical even coherent state ($\alpha = 2$). Mismatch parameters: $|\delta\Omega|/|\Omega| = \pm 0.1\%$ (dashed), and $|\delta\Omega|/|\Omega| = \pm 0.5\%$ (dotted), for the phase $\varphi = \pi/2$.

the exponential operators occurring in Eqs. (72)–(74) can be rewritten as

$$e^{i\hat{x}_\varphi \tau/2} = \hat{D}(i\tau e^{-i\varphi}/2). \tag{76}$$

Therefore the operators (72)–(74) can be expressed as superpositions of coherent displacements,

$$\langle 1|\hat{U}_{\mathrm{int}}(t)|1\rangle = \langle 2|\hat{U}_{\mathrm{int}}(t)|2\rangle = \frac{1}{2}\{\hat{D}^\dagger[\alpha(\tau;\varphi)] + \hat{D}[\alpha(\tau;\varphi)]\}, \tag{77}$$

$$\langle 1|\hat{U}_{\mathrm{int}}(t)|2\rangle = \frac{\Omega}{2|\Omega|}\{\hat{D}^\dagger[\alpha(\tau;\varphi)] - \hat{D}[\alpha(\tau;\varphi)]\}, \tag{78}$$

$$\langle 2|\hat{U}_{\mathrm{int}}(t)|1\rangle = \frac{\Omega^*}{2|\Omega|}\{\hat{D}^\dagger[\alpha(\tau;\varphi)] - \hat{D}[\alpha(\tau;\varphi)]\}, \tag{79}$$

where the coherent displacement amplitude is given by

$$\alpha(\tau;\varphi) = i\tau e^{-i\varphi}/2. \tag{80}$$

The full time evolution (25) determines the density operator after an interaction time t, where the ion is probed for resonance fluorescence. The probing for resonance fluorescence can be described by a projection on the electronic state $|1\rangle$ or $|2\rangle$, depending on the outcome of the probing [36,37]. Therefore the resulting motional density operator is conditioned on the outcome of the probing and reads as

$$\hat{\rho}^{(c)}(t) = \langle c|\hat{U}_0(t)\hat{U}_{\mathrm{int}}(t)\hat{\varrho}(0)\hat{U}_{\mathrm{int}}^\dagger(t)\hat{U}_0^\dagger(t)|c\rangle, \tag{81}$$

with $c = 1$ if one detects resonance fluorescence and $c = 2$ if no fluorescence signal can be detected. Note that in the case of $c = 1$ the motional state is disturbed by the light scattering, for $c = 2$ this effect is absent since no resonance fluorescence occurs. Due to the projection on the electronic levels, Eq. (81) can be simplified by using the free time evolution of the vibration (24), so that the conditioned density operator reads as

$$\hat{\rho}^{(c)}(t) = \hat{U}_{\mathrm{vib}}(t)\langle c|\hat{U}_{\mathrm{int}}(t)\hat{\rho}(0)\hat{\sigma}(0)\hat{U}_{\mathrm{int}}^\dagger(t)|c\rangle\hat{U}_{\mathrm{vib}}^\dagger(t). \tag{82}$$

With the initial electronic preparation (27), Eq. (82) can be related to the operators (77)–(79),

$$\hat{\rho}^{(c)}(t) = \sum_{a,b=1,2} \sigma_{ab}(0)\hat{U}_{\mathrm{vib}}(t)\langle c|\hat{U}_{\mathrm{int}}(t)|a\rangle\hat{\rho}(0) \times \langle b|\hat{U}_{\mathrm{int}}^\dagger(t)|c\rangle\hat{U}_{\mathrm{vib}}^\dagger(t). \tag{83}$$

By omitting the arguments of $\hat{D}[\alpha(\tau;\varphi)]$, one obtains for the conditioned motional quantum states the results

$$\hat{\rho}^{(1)}(t) = \hat{U}_{\mathrm{vib}}(t)\left[\frac{1+v}{4}\hat{D}\hat{\rho}(0)\hat{D}^\dagger + \frac{1-v}{4}\hat{D}^\dagger\hat{\rho}(0)\hat{D} - \frac{w-iu}{4}\hat{D}\hat{\rho}(0)\hat{D} - \frac{w+iu}{4}\hat{D}^\dagger\hat{\rho}(0)\hat{D}^\dagger\right]\hat{U}_{\mathrm{vib}}^\dagger(t), \tag{84}$$

and

$$\hat{\rho}^{(2)}(t) = \hat{U}_{\mathrm{vib}}(t)\left[\frac{1+v}{4}\hat{D}\hat{\rho}(0)\hat{D}^\dagger + \frac{1-v}{4}\hat{D}^\dagger\hat{\rho}(0)\hat{D} + \frac{w-iu}{4}\hat{D}\hat{\rho}(0)\hat{D} + \frac{w+iu}{4}\hat{D}^\dagger\hat{\rho}(0)\hat{D}^\dagger\right]\hat{U}_{\mathrm{vib}}^\dagger(t), \tag{85}$$

with the coefficients w, u, and v defined by the initial electronic preparation,

$$w = \sigma_{22}(0) - \sigma_{11}(0), \tag{86}$$

$$u = 2\mathrm{Re}[\sigma_{12}(0)e^{-i(\varphi_b+\varphi_r)/2}], \tag{87}$$

$$v = 2\mathrm{Im}[\sigma_{12}(0)e^{-i(\varphi_b+\varphi_r)/2}]. \tag{88}$$

From Eqs. (84) and (85) it can be seen that if the probing for resonance fluorescence is not performed, the interference terms of the two displaced components, $\hat{D}^\dagger\hat{\rho}(0)\hat{D}^\dagger$ and $\hat{D}\hat{\rho}(0)\hat{D}$, vanish and the resulting state is a statistical mixture of the two components. This can be shown by taking the electronic trace of the density operator,

$$\hat{\rho}(t) = \mathrm{Tr}[\hat{\varrho}(t)] = \hat{\rho}^{(1)}(t) + \hat{\rho}^{(2)}(t)$$
$$= \hat{U}_{\mathrm{vib}}(t)\left[\frac{1+v}{2}\hat{D}\hat{\rho}(0)\hat{D}^\dagger + \frac{1-v}{2}\hat{D}^\dagger\hat{\rho}(0)\hat{D}\right]\hat{U}^\dagger_{\mathrm{vib}}(t). \tag{89}$$

The back action of the measurement is rather simple when the ion is initially prepared in its electronic ground state $\sigma_{11}(0)=1$ ($w=-1$, $u=v=0$). The conditioned density operators after the probing for resonance fluorescence follow from Eqs. (84) and (85),

$$\hat{\rho}^{(1)}(t) = \hat{U}_{\mathrm{vib}}(t)\left[\frac{\hat{D}^\dagger+\hat{D}}{2}\right]\hat{\rho}(0)\left[\frac{\hat{D}^\dagger+\hat{D}}{2}\right]^\dagger \hat{U}^\dagger_{\mathrm{vib}}(t), \tag{90}$$

$$\hat{\rho}^{(2)}(t) = \hat{U}_{\mathrm{vib}}(t)\left[\frac{\hat{D}^\dagger-\hat{D}}{2}\right]\hat{\rho}(0)\left[\frac{\hat{D}^\dagger-\hat{D}}{2}\right]^\dagger \hat{U}^\dagger_{\mathrm{vib}}(t). \tag{91}$$

By appropriately choosing the interaction time τ, quantum superpositions of the initial motional quantum state with itself can be created. For example, if the ion is initially in a vibrational coherent state $|\alpha\rangle$, the two conditioned quantum states read as

$$|\psi^{(1)}(t)\rangle = \hat{U}_{\mathrm{vib}}(t)\frac{1}{2}[|\alpha+\alpha(\tau;\varphi)\rangle + |\alpha-\alpha(\tau;\varphi)\rangle], \tag{92}$$

$$|\psi^{(2)}(t)\rangle = \hat{U}_{\mathrm{vib}}(t)\frac{1}{2}[|\alpha+\alpha(\tau;\varphi)\rangle - |\alpha-\alpha(\tau;\varphi)\rangle]. \tag{93}$$

If $\alpha=0$, i.e., if the ion is initially laser-cooled to its vibrational ground state, then the resulting states are the even and odd coherent states [18]. Note that both even and odd coherent quantum superpositions can be created without disturbing effects due to light scattering by starting with the electronic states $|2\rangle$ and $|1\rangle$, respectively, and observing no resonance fluorescence signal. That is, to avoid disturbations due to light scattering it may be advantageous to change the electronic initial preparation by applying a π pulse on the electronic resonance.

A more complex situation for the preparation of quantum superposition states is shown in Fig. 9. The ion is initially prepared in a thermal state of motion of a mean thermal excitation $n_{\mathrm{th}}=1$. The superposition of this initial, completely incoherent state with itself gives rise to quantum interferences, which are clearly seen in the Wigner function. In Fig. 10 we show the Wigner function for a superposition of displaced number states. It displays the features of the Wigner function of each displaced number state, attaining already negative values, and of the quantum superposition

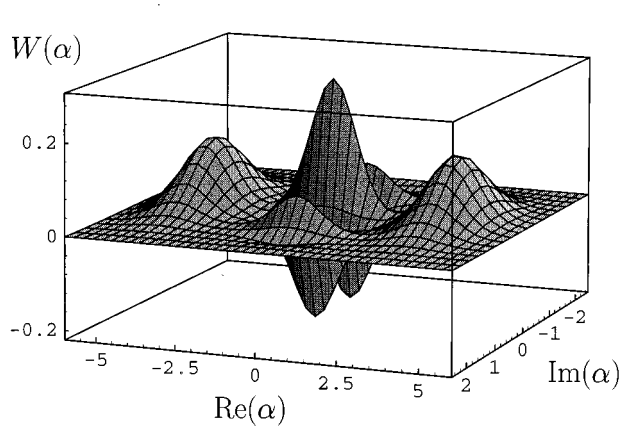

FIG. 9. Quantum superposition of two thermal states of $n_{\mathrm{th}}=1$ and coherent displacements of $\alpha=\pm 4$. Although the initial state is completely incoherent, the quantum superposition of the displaced components clearly exhibits interferences in the Wigner function, which are signatures of a nonclassical behavior.

with its pronounced interference fringes between the displaced number states. To produce states of this type, recent methods of preparing motional number states [20] could be readily combined with the measurement scheme under study. That is, besides the feasibility of measuring arbitrary quantum states of motion, our scheme is suited to create interesting quantum superpositions of the states to be measured. Subsequently, the created states could be measured by the same technique. Clearly, this procedure could be repeated several times in order to create a variety of complex quantum superposition states.

VI. SUMMARY AND CONCLUSIONS

In conclusion, we have shown that the full information on the quantum mechanical state of a trapped ion can be obtained from the dynamics of the ground-state occupation probability of a long-living electronic transition. To achieve this, the transition is irradiated by two lasers, tuned to the

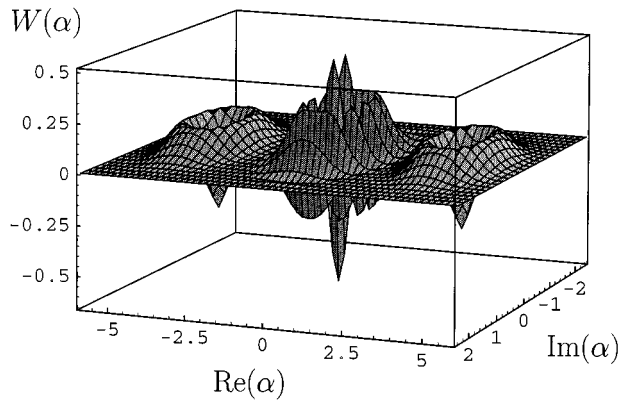

FIG. 10. Quantum superposition of two number states $|1\rangle$ with coherent displacements of $\alpha=\pm 4$. The quantum superposition of the displaced components clearly exhibits interferences in the Wigner function, which are signatures of a nonclassical behavior.

well resolved upper and lower vibrational sidebands. The intensities of the two laser fields are matched in such a manner that the couplings of both transitions (described by the vibronic Rabi frequencies) are equal. In this case, the interaction Hamiltonian describing the coupling between the moving ion and the two lasers corresponds to the coupling between a two-level system and a classical light field, multiplied by the phase-dependent, generalized position operator of the ionic center-of-mass motion. This interaction transforms the full information on the motional quantum state into the occupation dynamics of the electronic ground state, which directly yields the characteristic function of the phase-dependent, generalized spatial distribution.

The occupation of the electronic ground state is readily observed by switching on a laser, driving a second, strong transition of the ion. Only when the ion is in its electronic ground state does this lead to the onset of resonance fluorescence. The ground-state occupations, measured as a function of the interaction time of the two lasers driving the weak transition, allow to determine the desired information on the motional quantum state. Explicit results have been derived, relating the time-dependent fluorescence signals to the density matrices in both a generalized position representation and a number-state representation. Since the test for fluorescence on a strong transition is highly efficient, the method is almost free of the limitations due to nonideal detection known from other methods of measuring quantum states.

Our method allows one to record a well defined, ultimate classical noise level for the motion of the ion. A reference measurement of the fluorescence signal of an ion laser-cooled to its vibrational ground state may serve as a boundary between classical and nonclassical behavior of the quantum state under study. Typical nonclassical quantum states, such as number states or quantum superposition states, show a fluorescence dynamics on a time scale that is longer than the corresponding dynamics of the laser-cooled ion. That is, nonclassical effects are easily measured as a slowly decaying long-time dynamics, instead of giving rise to sharp structures in measured distributions that are easily smoothed out. This is an advantage due to the fact that the method allows to directly observe the characteristic functions rather than the corresponding spatial distributions. We have considered the effects of imperfect matching of the intensities of the lasers irradiating the weak transition. These effects modify the long-time dynamics and can be used to calibrate the matching of the laser intensities, by using a laser-cooled ion and adjusting the intensities in order to suppress the long-time dynamics of the fluorescence signal.

Moreover, we have studied the back action of the measurement procedure on the motional quantum state. The simplicity of the interaction Hamiltonian allows one to exactly solve this problem. It turns out that the interaction dynamics on the weak transition effectively leads to a simultaneous displacement of the state to be measured into two opposite directions in phase space. The probing for resonance fluorescence disentangles the vibronic quantum state, thereby reducing the motional quantum state to a quantum superposition of two displaced replica of the motional state to be measured. Thus, our measurement scheme allows one to create Schrödinger-cat-like quantum superpositions of the initial state, displaced in two opposite directions in phase space. Thereby, interesting quantum interferences can be produced from completely incoherent states. For example, quantum superpositions of thermal states and of number states are considered. Our scheme allows one to produce and detect such interesting quantum states by the same technique. Repeating this procedure allows one to create a variety of motional quantum states exhibiting rich structures in phase space, connected with strong quantum interference effects.

Note added in proof: After submission of this paper we became aware of some other contributions concerning the measurement of motional quantum states of trapped ions; cf. C. D'Helon and G. J. Milburn, Phys. Rev. A **54**, R25 (1996); P. J. Bardroff, C. Leichtle, G. Schrade, and W. P. Schleich, Phys. Rev. Lett. **77**, 2198 (1996); D. Leibfried, D. M. Meekhof, B. E. King, C. Monroe, W. M. Itano, and D. J. Wineland (unpublished).

ACKNOWLEDGMENTS

The authors gratefully acknowledge valuable discussions with C. Monroe, P.E. Toschek, and D.J. Wineland. This research was supported by the Deutsche Forschungsgemeinschaft.

[1] W. Neuhauser, H.G. Dehmelt, and P.E. Toschek, Phys. Rev. A **22**, 1137 (1980).
[2] W. Nagourney, J. Sandberg, and H.G. Dehmelt, Phys. Rev. Lett. **56**, 2797 (1986).
[3] Th. Sauter, W. Neuhauser, R. Blatt, and P.E. Toschek, Phys. Rev. Lett. **57**, 1696 (1986).
[4] J.C. Bergquist, R.G. Hulet, W.M. Itano, and D.J. Wineland, Phys. Rev. Lett. **57**, 1699 (1986).
[5] H.J. Kimble, M. Dagenais, and L. Mandel, Phys. Rev. Lett. **39**, 691 (1977).
[6] F. Diedrich and H. Walther, Phys. Rev. Lett. **58**, 203 (1987).
[7] M. Schubert, I. Siemers, R. Blatt, W. Neuhauser, and P.E. Toschek, Phys. Rev. Lett. **68**, 3016 (1992).
[8] W. Vogel, Phys. Rev. Lett. **67**, 2450 (1991); Phys. Rev. A **51**, 4160 (1995).
[9] D.F. Walls and P. Zoller, Phys. Rev. Lett. **47**, 709 (1981).
[10] A more detailed treatment includes the micromotion; see L.S. Brown, Phys. Rev. Lett. **66**, 527 (1991); R.J. Glauber, in *Foundations of Quantum Mechanics*, edited by T.D. Black, M.M. Nieto, H.S. Pilloff, M.O. Scully, and R.M. Sinclair (World Scientific, Singapore, 1992), p. 23; K.H. Yeon, H.J. Kim, C.I. Um, T.F. George, and L.N. Pandey, Phys. Rev. A **50**, 1035 (1994); A. Lindner, Z. Phys. D **33**, 43 (1995). Experimentally the micromotion can be reduced [see Ref. [7]; S.R. Jefferts, C. Monroe, E.W. Bell, and D.J. Wineland, Phys. Rev. A **51**, 3112 (1995)] so that the harmonic approximation is suitable.
[11] F. Diedrich, J.C. Bergquist, W.M. Itano, and D.J. Wineland, Phys. Rev. Lett. **62**, 403 (1989).
[12] C. Monroe, D.M. Meekhof, B.E. King, S.R. Jefferts, W.M. Itano, and D.J. Wineland, Phys. Rev. Lett. **75**, 4011 (1995).

[13] D.J. Heinzen and D.J. Wineland, Phys. Rev. A **42**, 2977 (1990).
[14] J.I. Cirac, A.S. Parkins, R. Blatt, and P. Zoller, Phys. Rev. Lett. **70**, 556 (1993); J.I. Cirac, A.S. Parkins, R. Blatt, and P. Zoller, *ibid.* **70**, 762 (1993).
[15] H.P. Zeng and F.C. Lin, Phys. Rev. A **48**, 2393 (1993).
[16] H.P. Zeng and F.C. Lin, Phys. Rev. A **52**, 809 (1995).
[17] R.L. de Matos Filho and W. Vogel, Phys. Rev. A **50**, R1988 (1994).
[18] R.L. de Matos Filho and W. Vogel, Phys. Rev. Lett. **76**, 608 (1996).
[19] R.L. de Matos Filho and W. Vogel, Phys. Rev. A (to be published).
[20] D.M. Meekhof, C. Monroe, B.E. King, W.M. Itano, and D.J. Wineland, Phys. Rev. Lett. **76**, 1796 (1996).
[21] C. Monroe, D.M. Meekhof, B.E. King, and D.J. Wineland, Science **272**, 1131 (1996).
[22] C.A. Blockley, D.F. Walls, and H. Risken, Europhys. Lett. **17**, 509 (1992).
[23] W. Vogel and R.L. de Matos Filho, Phys. Rev. A **52**, 4214 (1995).
[24] D.T. Smithey, M. Beck, M.G. Raymer, and A. Faridani, Phys. Rev. Lett. 70, 1244 (1993). For the underlying theory see K. Vogel and H. Risken, Phys. Rev. A **40**, 2847 (1989). For an alternative approach to determine directly the quasiprobability distributions see S. Wallentowitz and W. Vogel, *ibid.* **53**, 4528 (1996).
[25] T.J. Dunn, I.A. Walmsley, and S. Mukamel, Phys. Rev. Lett. **74**, 884 (1995).
[26] S. Wallentowitz and W. Vogel, Phys. Rev. Lett. **75**, 2932 (1995).
[27] P.E. Toschek, Ann. Phys. (Paris) **10**, 761 (1985); M. Lindberg and J. Javanainen, J. Opt. Soc. Am. B **3**, 1008 (1986).
[28] P.E. Toschek (private communication).
[29] An alternative approach to measure the quantum state beyond the Lamb-Dicke regime has been proposed by J.F. Poyatos, R. Walser, J.I. Cirac, and P. Zoller, Phys. Rev. A **53**, R1966 (1996). It requires fast switchings of both the coherent excitation and the trap frequency, the latter by at least two orders of magnitude. Besides technical stability problems in such a method, in principle only a smoothed distribution can be reconstructed since the squeezing does not yield a perfect measurement of the generalized position as in our scheme. Note that both more significant and more stable squeezing could be achieved by the methods used in Ref. [20].
[30] M. Schubert and W. Vogel, Wiss. Z. Univ. Jena, Math.-Naturwiss. Reihe **27**, 179 (1978); see also W. Vogel and D.-G. Welsch, *Lectures on Quantum Optics* (Akademie Verlag, Berlin, 1994), Sec. 3.4.
[31] This electronic preparation is a pure state, which can be described by coefficients $\sigma_{ab}(0)=c_a c_b^*$. Nevertheless, also nonpure quantum states can be prepared to get the desired antisymmetrized spatial distribution. This only decreases the measurable fluorescence signal.
[32] H. Kühn, D.-G. Welsch, and W. Vogel, J. Mod. Opt. **41**, 1607 (1994).
[33] G.M. D'Ariano, C. Macchiavello, and M.G.A. Paris, Phys. Rev. A **50**, 4298 (1994); Phys. Lett. A **195**, 31 (1994); G.M. D'Ariano, U. Leonhardt, and H. Paul, Phys. Rev. A **52**, R1801 (1995); U. Leonhardt, H. Paul, and G.M. D'Ariano, *ibid.* **52**, 4899 (1995).
[34] *Handbook of Mathematical Functions*, edited by M. Abramowitz and I. A. Segun (Dover Publications, New York, 1972).
[35] Th. Richter, Phys. Lett. A **211**, 327 (1996).
[36] R.G. Hulet, D.J. Wineland, J.C. Bergquist, and W.M. Itano, Phys. Rev. A **37**, 4544 (1988).
[37] A. Beige and G.C. Hegerfeldt, Phys. Rev. A **53**, 53 (1996).